IEEE Access
Multidisciplinary | Rapid Review | Open Access Journal

Received July 12, 2021, accepted July 18, 2021, date of publication July 20, 2021, date of current version August 5, 2021.

Digital Object Identifier 10.1109/ACCESS.2021.3098925

Solving the Magnetocardiography Forward Problem in a Realistic Three-Dimensional Heart-Torso Model

ZHENGHUI HU, KAIKAI YE, MINGZHU BAI, ZEKUAN YANG, AND QIANG LIN
College of Science, Zhejiang University of Technology, Hangzhou 310023, China

Corresponding author: Zhenghui Hu (zhenghui@zjut.edu.cn)

This work was supported in part by the National Key Research and Development Program of China under Grant 2018YFA0701400, and in part by the Public Projects of Science Technology Department of Zhejiang Province under Grant LGF20H180015.

This work involved human subjects or animals in its research. Approval of all ethical and experimental procedures and protocols was granted by the Research Ethics Committee of the College of Science, Zhejiang University of Technology.

ABSTRACT The forward problem in magnetocardiography (MCG) is important for understanding the relationship between the electric activity of the heart and the body surface magnetic field (BSM), and providing insight into the clinical application of MCG. In this paper, we proposed a computational framework based on the finite element method (FEM) to solve the MCG forward problem. For the subject-specific heart-torso geometry established from the medical image, the modified FitzHugh-Nagumo (FHN) equation was used to describe the volumetric myocardial dynamic transmembrane potential (TMP), then the quasi-static Maxwell equations was applied to simulate the propagation of cardiac magnetic field produced by TMP. The two parts were validated on the simplified one-dimensional FHN equation and the source model of the straight wire respectively, in which the analytical solutions exist. Further, under a realistic geometry heart-torso model, the distribution of the body surface magnetic vector field was presented, the component in the direction perpendicular to the body surface (B_y) of which was in very good agreement with the actual observations from the same subject on a pulse-pumped Rb atomic magnetometer.

INDEX TERMS Magnetocardiography (MCG), forward problem, fitzhugh-nagumo (FHN) equation, transmembrane potential (TMP), body surface magnetic field (BSM).

I. INTRODUCTION

Cardiovascular disease seriously affects human health [1], and hence its early diagnosis is important. Electrocardiography (ECG) and magnetocardiography (MCG) are currently two techniques used to detect cardiac electrophysiological activity. However, due to the different physical characteristics of cardiac electromagnetic fields, the information provided by the two is also different [2]. The propagation of electric field in the heart will be refracted, scattered, and absorbed due to the inhomogeneous distribution of the conductivity and permittivity of human tissues [3], resulting in the electric field being projected nonlinearly onto the body surface (i.e., as detected using ECG). In contrast, the magnetic field is projected linearly onto the body surface (i.e., as detected using MCG), which is due to the magnetic permeability of the tissues changing very little, and it is usually regarded as a constant value approximately equal to that in a vacuum. Thus, MCG may be more helpful than ECG in diagnosing heart disease, because the magnetic field measured by MCG is a vector, which contains more detailed cardiac electrophysiological information than the electric field measured by ECG [4].

One major problem for MCG is that the strength of the cardiac magnetic field is about one-millionth of the geomagnetic field [5], which makes it very difficult to measure accurately. Since the discovery of high-temperature superconductors, superconducting quantum interference device (SQUID) magnetometers have been used to measure weak biological magnetic fields [6]. However, SQUID magnetometers are unsuitable for clinical applications of MCG, because they must be kept at low temperature with liquid helium in a vacuum dewar container, which is characterized by high maintenance charge and manufacturing costs. Recently,

The associate editor coordinating the review of this manuscript and approving it for publication was Rajeswari Sundararajan.

the rapid development of atomic magnetometers is making them show superior performance in measuring weak magnetic fields [7]. Our research group has carried out related work with atomic magnetometers, and we have developed a pulse-pumped Rb atomic magnetometer [8], [9] that can successfully measure MCG signals from three different directions at room temperature.

Many studies have been devoted to the ECG forward problem, but relatively little to the MCG forward problem. Shou *et al.* have proposed that the equivalent double layer (EDL) source model is helpful for the MCG research, and then they used an electrodynamic heart model to simulate the MCG, taking the conductivity of lung into account [10], [11]. Alday *et al.* have presented a membrane model to compare the ECG and MCG under myocardial ischemia in 2015, the results showed that MCG is more sensitive to ischemia than ECG [12]. In the work of Bhat and Anitha, the discretized heart has been assumed as a dipolar sources forming a double layer, and then a uniform double layer model representing the transmembrane distribution on the epicardium and endocardium was used to simulate the MCG [13]. Solving the MCG forward problem not only provides prior knowledge for the subsequent MCG inverse problem, but also helps to obtain a deep understanding of the mechanisms underlying heart disease. Therefore, further research on the MCG forward problem is likely to be very fruitful.

This paper presents a computational framework for the MCG forward problem based on a personalized three-dimensional (3D) heart-torso model to study the body surface magnetic field (BSM) generated by cardiac excitation. We segmented the MRI images of the subject to separate the cardiac chambers and the torso, and then personalized 3D geometric models of the human heart and torso were reconstructed from the processed images. On the basis of these models, the modified FitzHugh-Nagumo (FHN) equation was used to establish a cardiac electrophysiological model to obtain the excitation conduction process of the TMP in the heart. After that, a cardiac magnetic field model for the body surface was also established based on the quasi-static Maxwell equations [14], and combined with the cardiac electrophysiological model to study the diffusion of the magnetic field generated by the TMP in the torso, and then the projection distribution of the BSM was obtained.

The calculation process used in this study was based on the Galerkin finite element method (FEM). The accuracy of the computational framework was verified by comparing the FEM solution and the analytical solution on the simplified cardiac electrophysiological model and the cardiac magnetic field model. Finally, the simulated MCGs were compared with actual MCGs measured using a pulse-pumped Rb atomic magnetometer developed independently by our laboratory. The results have demonstrated that the computational framework is feasible.

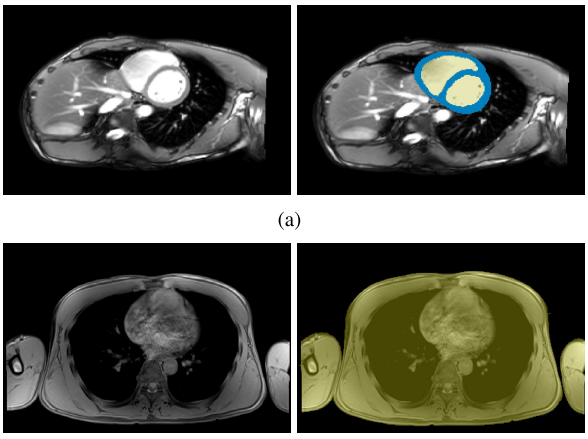

(a)

(b)

FIGURE 1. Images of MRI slices. (a) Image segmentation of the heart and contour division of the atrium and ventricle. (b) Image segmentation of the torso.

II. MODELS AND METHODS

A. THREE-DIMENSIONAL HEART-TORSO MODEL

A 3D personalized heart–torso model was established to study the physical connection between the cardiac TMP and BSM. Traditional 3D cardiac data sources from anatomical models such as canines have limitations since they differ markedly from the geometry of the real human body. Noninvasive human medical tomography methods such as computed tomography and MRI allow us to obtain images from subjects, and then generated the personalized 3D heart-torso model by 3D reconstruction. Compared with the model obtained from anatomy, the model reconstructed from the tomographic scan lacks the information of the fiber structures of the personalized heart model. The initial phase of this study did not consider the fiber structures of the personalized heart model.

The 3D geometric model was based on the MRI data of a 25 years old healthy male subject. The heart model was reconstructed from 18 MRI images with 118 $\times$ 208 pixels, 1 mm $\times$ 1 mm resolution and 10 mm tomographic resolution. The torso model was based on 72 MRI images with 189 $\times$ 384 pixels, 1 mm $\times$ 1 mm resolution and 4 mm tomographic resolution. According to the gray value of MRI, threshold segmentation was performed to obtain binary images for determining the basic contours of the heart and torso. 3D image reconstruction was then applied to the processed images, and the reconstructed 3D geometry was smoothed appropriately without affecting the structure of heart and torso to eliminate the surface roughness in the process of image segmentation [15], [16], as shown in Figure 2.

B. CARDIAC ELECTROPHYSIOLOGICAL DIFFUSION MODEL

The Aliev-Panfilov model used in this study is a modified FitzHugh-Nagumo (FHN) model [17], [18]. The original FHN model is composed of nonlinear partial

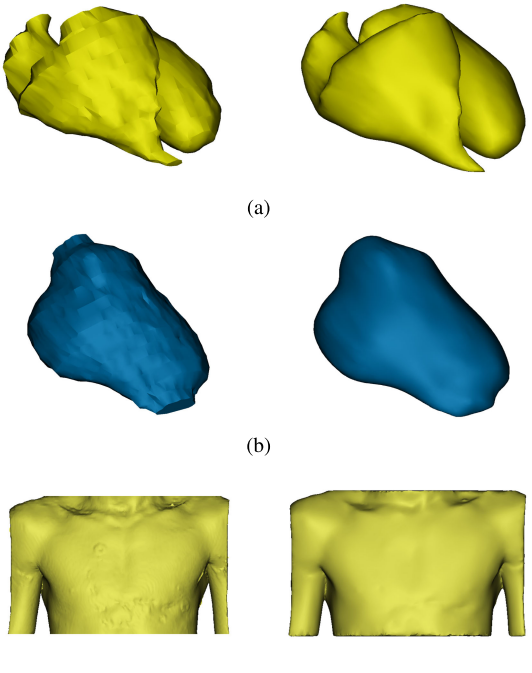

FIGURE 2. 3D reconstructed model (Left) and smoothed model (Right). (a) Endocardium. (b) Epicardium. (c) Torso.

differential equations

$$\begin{cases} \dfrac{\partial u}{\partial t} = \nabla \cdot (\mathbf{D}\nabla u) + f_1(u, v), \\ \dfrac{\partial v}{\partial t} = f_2(u, v), \end{cases} \tag{1}$$

where $f_1(u, v) = u(u - a)(1 - u) - v, f_2(u, v) = b(u - dv)$, and u stands for TMP (the activator variable), ranging from 0 to 1, and v for gate variable (the inhibitor variable). The activator variable u corresponds to the electric potential, and the inhibitor v is a variable that describes the voltage-dependent probability of the pores in the membrane being open and ready to transmit ionic current. And $\nabla \cdot (\mathbf{D}\nabla u)$ for diffusion term, D for diffusion tensor. Different $f_1(u, v)$ and $f_2(u, v)$ result in different TMP shapes.

The Aliev and Panfilov model was defined as:

$$\begin{cases} \dfrac{\partial u}{\partial t} = \nabla \cdot (\mathbf{D}\nabla u) + ku(u - a)(1 - u) - uv, \\ \dfrac{\partial v}{\partial t} = -e(v + ku(u - a - 1)), \end{cases} \tag{2}$$

where $a = 0.15$, $e = 0.01$, $k = 8$ [19], we assume that the myocardium is isotropic (i.e., $\mathbf{D} = 1$). The model involves dimensionless variables u, v and t. The actual TMP V_m and time t can be obtained with the formulas [17]:

$$V_m[mV] = 100u - 80, \quad t[ms] = 12.9t. \tag{3}$$

The actual TMP ranges from $-80\,mV$ to $20\,mV$. The heart is generally considered to be an isolated continuum, in which no active current flows into or out of the heart. There exists Neumann's condition $\partial u/\partial \mathbf{n} = 0$ when solving problems with boundaries, where $\mathbf{n}$ is the normal vector of cardiac boundary.

C. CARDIAC MAGNETIC FIELD MODEL

Since the electromagnetic field frequency of the human heart is about 1-100 Hz [20], this low frequency electromagnetic field is usually analyzed using the quasi-static Maxwell equations. The external magnetic field results from the current density generated by TMP in the heart. And the MCG signal is the projected integral of the magnetic field of the heart outside the body. The external current density in the heart J^i and TMP satisfy the following formula:

$$J^i = \sigma_H \nabla V_m, \tag{4}$$

where σ_H represents conductivity of heart tissues. Since the heart and torso were regarded as volume conductors, the total current density J in the model is the sum of the external current density and the passive volume current density:

$$J = -\sigma \nabla \varphi + J^i, \tag{5}$$

where σ represents conductivity, φ represents potential. The current density J satisfies the law of conservation of current [21]:

$$\nabla \cdot J = 0. \tag{6}$$

Since the MCG problem satisfies the quasi-static magnetic field, variation of magnetic field caused by variation of electric field can be ignored. Then the magnetic induction intensity B can be easily obtained by coupling the TMP to the quasi-static Maxwell equations:

$$\nabla \times B = \mu(-\sigma \nabla \varphi + J^i), \tag{7}$$

where μ is magnetic permeability. Since human tissues are nonmagnetic, the relative magnetic permeability $\mu_r = 1$, so $\mu = \mu_0\mu_r = \mu_0$, and the differential equation of the Magnetic vector potential A can be obtained since it meets $B = \nabla \times A$ and also satisfies the Coulomb gauge,

$$\nabla^2 A = -\mu_0 J. \tag{8}$$

Thus, we calculated A in the heart region and torso region respectively as:

$$\nabla^2 A = -\mu_0(-\sigma_H \nabla \varphi + J^i), \tag{9}$$

$$\nabla^2 A = -\mu_0(-\sigma_T \nabla \varphi), \tag{10}$$

where σ_T stands the torso conductivity, due to the tiny air conductivity Ω_A, the current outside torso is negligible. We calculated A in the air region as:

$$\nabla^2 A = 0. \tag{11}$$

According to the electromagnetic theory, the propagation of the magnetic field on the heart surface Γ_H and on the torso surface Γ_T are both satisfy the following boundary conditions: $B_{1n} = B_{2n}$ (magnetic induction intensity is equal in the normal direction), $H_{1t} = H_{2t}$ (magnetic field intensity is equal in the tangent direction).

D. FINITE ELEMENT CALCULATION

The boundary element method (BEM) [22], FEM [23], and mesh-free method [24] have been used to solve the partial differential equations and physical field problems with complex boundaries. However, considering that FEM is better than BEM at dealing with problems with complex boundaries, since it divides a complex model into many smaller finite elements, FEM was adopted in this paper to investigate the MCG forward problem. Due to the wider practical range of the weak form of the equivalent integral, the Galerkin version of the weighted remainder method was applied to calculate the reaction–confusion equation and the quasi-static magnetic field of the model.

A second-order 10-node tetrahedral element was adopted to discretize the heart, torso, and air domain. A second-order Lagrangian element was adopted for the function of element shape, which can simulate the curved boundary with higher calculation accuracy. The TMP distribution was determined using the Galerkin method and applied to the cardiac magnetic field model on the body surface, and then the BSM distribution was obtained.

A tetrahedral mesh was applied to the model for further FEM calculations, as shown in Figure 3. A dense tetrahedron mesh was used for the heart and a relatively sparse mesh was used for the torso to make the simulations more realistic while reducing the computation cost. The heart, torso, and air domain comprised 161,211, 7,907, and 2,584 tetrahedral units, respectively (the air domain is not shown in the figure).

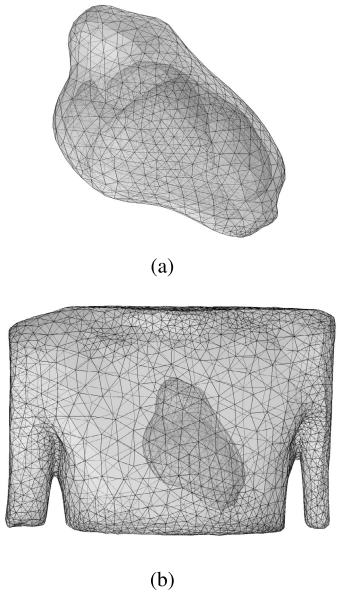

(a)

(b)

FIGURE 3. Discretized three-dimensional heart-torso model. (a) 3D cardiac model. (b) Heart-torso model.

Sine the sinoatrial (SA) node is the principal pacemaker of the heart [25], we defined the initial condition as an initial potential distribution u, where there was a constant elevated potential u_0 near the SA node (in our work, $u_0 = 1$), while the potential of the rest of the heart was 0, as shown in Figure 4. For the inhibitor variable v, it set as 0 near the SA node, and the rest of the potential was v_0 (in our work, $v_0 = 0.3$).

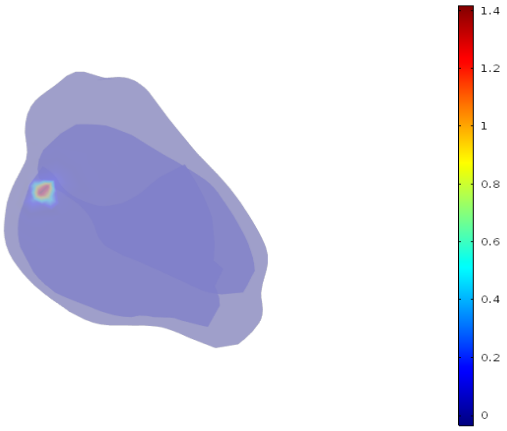

FIGURE 4. The result of a brief evolution of initial potential distribution u.

E. ANALYTICAL SOLUTION VALIDATION

To verify the reliability of the FEM calculation results and calculate the error between analytical solution and numerical solution. We considered the one-dimensional (1D) FHN equation to easily obtain the analytical solution of the FHN model and compared it with the Galerkin finite element numerical solution under the same condition. In the FHN equation (1), parameter b satisfies $0 < b \ll 1$, then v is a constant and can be assumed to 0. The FHN equation can be simplified to a nonlinear reaction-confusion equation:

$$\frac{\partial u}{\partial t} = \mathbf{D}\frac{\partial^2 u}{\partial x^2} + u(u-a)(1-u). \tag{12}$$

Relevant studies show that analytical solutions of nonlinear equations can be obtained through homogeneous equilibrium method [26], tanh method [27], variable coefficient Bernoulli auxiliary method [28], etc. The tanh method was applied in this study. We supposed the traveling wave solutions to (12) exists, let $u(x,t) = u(\xi)$, where $\xi = k(x - ct)$, and transformed the equation into the ordinary differential equation of $u(\xi)$. Put $Y = tanh^2\xi$ into $\frac{du}{d\xi} = 1 - Y^2$, then the homogeneous equation about Y was obtained by using the homogeneous balance. Assuming that the coefficient of the equation is 0, several traveling wave solutions can be obtained.

To verify the accuracy of the numerical solution of the BSM, a simple geometric model was established and the analytical solution of the magnetic field was solved based on the Maxwell equations. Researchers usually simulate the magnetic field generated by the heart by solving the magnetic field produced by a magnetic dipole, but it is a poor approximation of the electrophysiological activity of the heart. Wang *et al.* [29] have applied a concentric sphere model to study the cardiac potential distribution, the mechanism of which is somewhat similar to that of the heart. An inner concentric sphere was used to simulate the heart, and we assume

that J^i in the inner sphere is evenly distributed vertically upward. The magnetic induction intensity in the model have been first given by Geselowitz [21]:

$$B = \frac{\mu_0}{4\pi}[\int J^i \times \nabla(\frac{1}{R})dv - \sum \sigma \nabla V \times \nabla(\frac{1}{R})dv]. \quad (13)$$

Due to the symmetry, there is no component of the magnetic field in the r and z directions. That is, in the cylindrical coordinate system, the magnetic field generated by the inner-sphere current is in the φ direction, which is consistent with that of the magnetic field generated by a finite length current-carrying straight conductor. Assuming that the straight conductor with length L, current I equivalently contributes to the magnetic field generated by the inner sphere current, and suppose that the electric conductivity of outer sphere $\sigma_T \ll 1$. The magnetic induction intensity of the simplified model can be defined as:

$$B = \frac{\mu_0}{4\pi} \int_L \frac{Id\vec{l} \times R}{R^3}, \quad (14)$$

where R is the vector from field point $r = re_r + ze_z$ to source point $r' = z'e_z$,

$$B = e_\varphi \frac{\mu_0 I}{4\pi r} \frac{z - z'}{[r^2 + (z - z')^2]^{1/2}} \Big|_{z'=-L/2}^{z'=L/2}. \quad (15)$$

III. SIMULATION AND EXPERIMENT

A. VALIDATION OF CARDIAC ELECTROPHYSIOLOGICAL DIFFUSION MODEL

Through the tanh method, fifteen traveling wave solutions of 1D FHN equation were obtained, and one of them was taken as an example below.

$$u(x, t) = \frac{1}{2} - \frac{1}{2}\tanh[\frac{x}{2\sqrt{2D}} + \frac{1}{4}(2a - 1)t]. \quad (16)$$

Using $t = 0$ of (16) as the initial value of (12), the numerical solution by FEM under 1D condition was obtained and compared with the analytical solution under the same condition to verify the accuracy of the Galerkin method under 1D condition. The relative root mean squared error *RRMSE* was defined as:

$$RRMSE = \sqrt{\frac{\sum_N (b_n - a_n)^2}{\sum_N (a_n)^2}} \times 100\%, \quad (17)$$

where a_n is the analytical solution, b_n is the numerical solution, N is the total time step or computing node of a numerical solution.

Figure 5 displays the evolution of excitation potential u of analytical and numerical solutions. The *RRMSE* between the analytical solution and the corresponding numerical solution of the simplified FHN equation are 0.60%, 0.91%, and 0.61% respectively, as shown in Table 1. The results show that the error between the numerical solution of the simplified FHN equation obtained by the Galerkin method under 1D condition and the analytical solution obtained by the tanh method is small, indicating the electrophysiological model is credible.

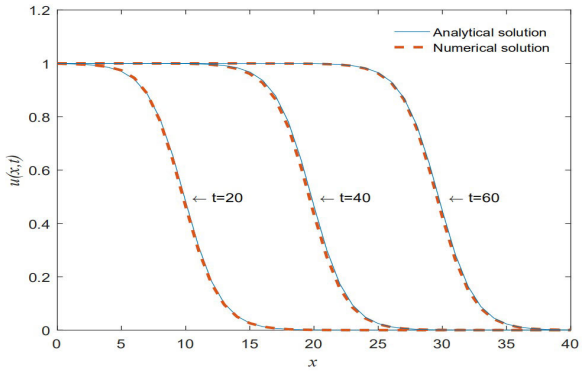

FIGURE 5. Evolution of excitation potential u at t = 20, 40, 60 (left to right). Solid line: analytical solution of FHN equation. Dotted line: numerical solution of FHN equation.

TABLE 1. RRMSE of 1D FHN equation.

time	t=20	t=40	t=60
RRMSE	0.60%	0.91%	0.61%

As a small cluster of pacemaker cells, the SA node stimulates the action potential and propagates TMP. Thus, the action potential $u = 1$ was set as the initial condition of the FHN equation to stimulate the propagation of TMP. Then the dynamic TMP can be obtained through FEM calculation. Figure 6 illustrates the distribution of TMP in ventricular excitation, and the TMP evolution curve over time is shown in Figure 7, which is basically consistent with the evolution curve of TMP over time under normal heart rate. [30], indicating that the modified FHN equation used as the cardiac source diffusion equation is consistent with the electrical excitation diffusion characteristics of the actual heart.

B. SIMULATION OF BODY SURFACE MAGNETIC FIELD

In Figure 8, the distribution of the magnetic field on the plane generated by a current-carrying straight conductor with finite length is presented. Here the long straight conductor represents the source of the heart and the magnetic field distribution on the plane represents the BSM. Figure 9 illustrates the changes of the norm of magnetic induction intensity over the vertical distance between the field point and the conductor. It can be seen that the error between the numerical solution and the analytical solution is small, indicating the accuracy of the numerical solution of the FEM.

The anisotropic conductivity of the 3D heart wall model should be taken into account for better simulation. Since bulk conductivity counts for little to the propagation of MCG signal, it can be assumed as isotropic. Heart conductivity was chosen: $\sigma_H = 0.48$[S/m]; bulk conductivity was chosen: $\sigma_T = 0.2$[S/m] [31], without considering the myocardial

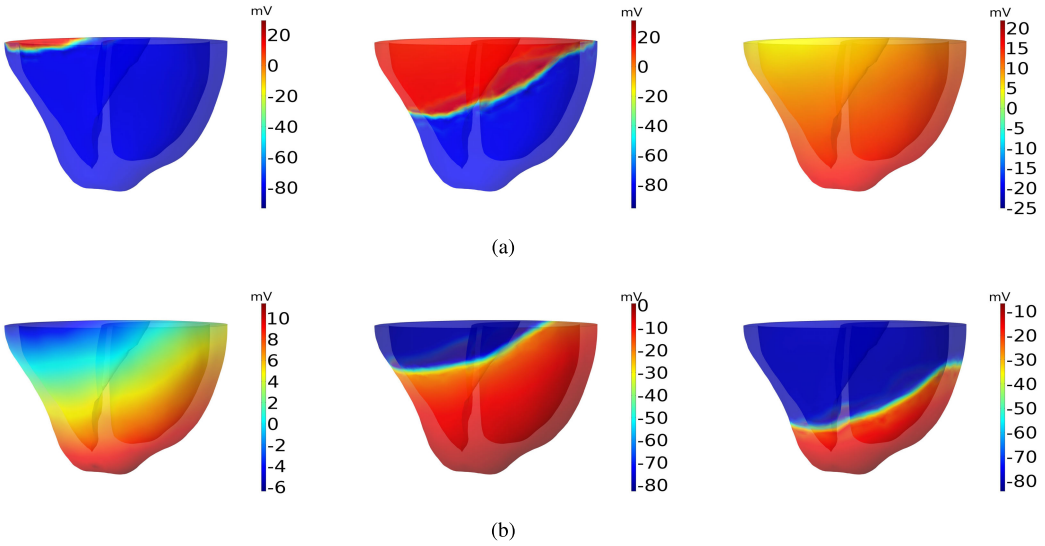

FIGURE 6. The TMP distribution in a cardiac cycle. (a) Depolarization process (left to right: t = 30, 60, 90). (b) Repolarization process (left to right: t = 120, 150, 180).

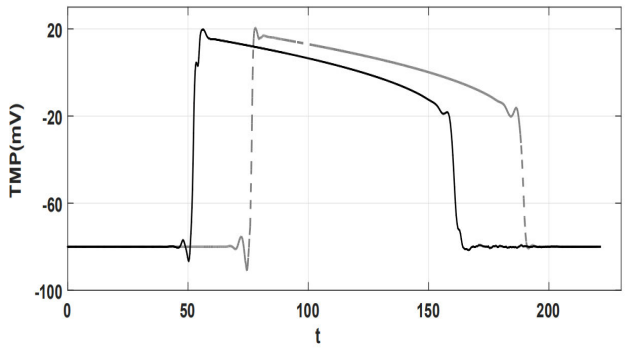

FIGURE 7. TMP time evolution curve. Solid line: right ventricular TMP. Dotted line: left ventricular TMP.

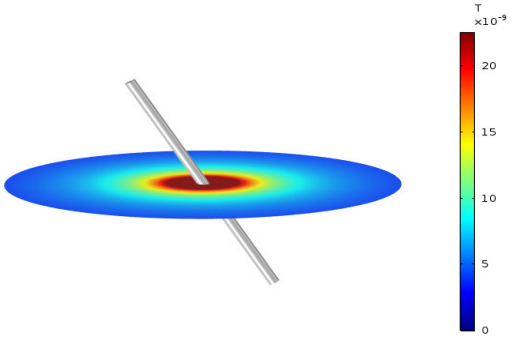

FIGURE 8. The distribution of magnetic field on the axial plane of straight wire model.

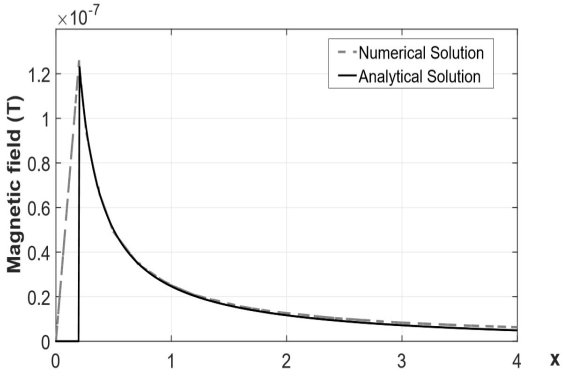

FIGURE 9. Distribution of magnetic field on the axial plane. *x* denotes the vertical distance from the field point to the wire. Solid line: numerical solution. Dotted line: analytical solution.

fiber orientation. A detection sensor was simulated about 5mm in front of the chest. By applying the cardiac electrophysiological model to the static cardiac magnetic model, the magnetic induction intensity distribution over time in the detection surface was obtained. Figure 10 displays the BSM distributions at four moments during cardiac depolarization and repolarization.

To further verify the feasibility of the computational framework, a set of actual MCGs were compared with simulated MCGs, the heart data were obtained from a 25 years old healthy man, measured perpendicular to the body surface (B_y) under our self-developed pulse-pumped Rb atomic magnetometer, and the MCGs were plotted every 20ms by linear interpolation during depolarization and repolarization, as shown in Figure 11. Then, we used the structural similarity index (SSIM) [32] to evaluate the similarity between the simulated MCGs and the measured MCGs. The SSIM defines the structure information as independent of brightness and contrast from the perspective of image composition, which reflects the structural properties of objects in the scene. The mean value is used as the brightness estimation, the standard

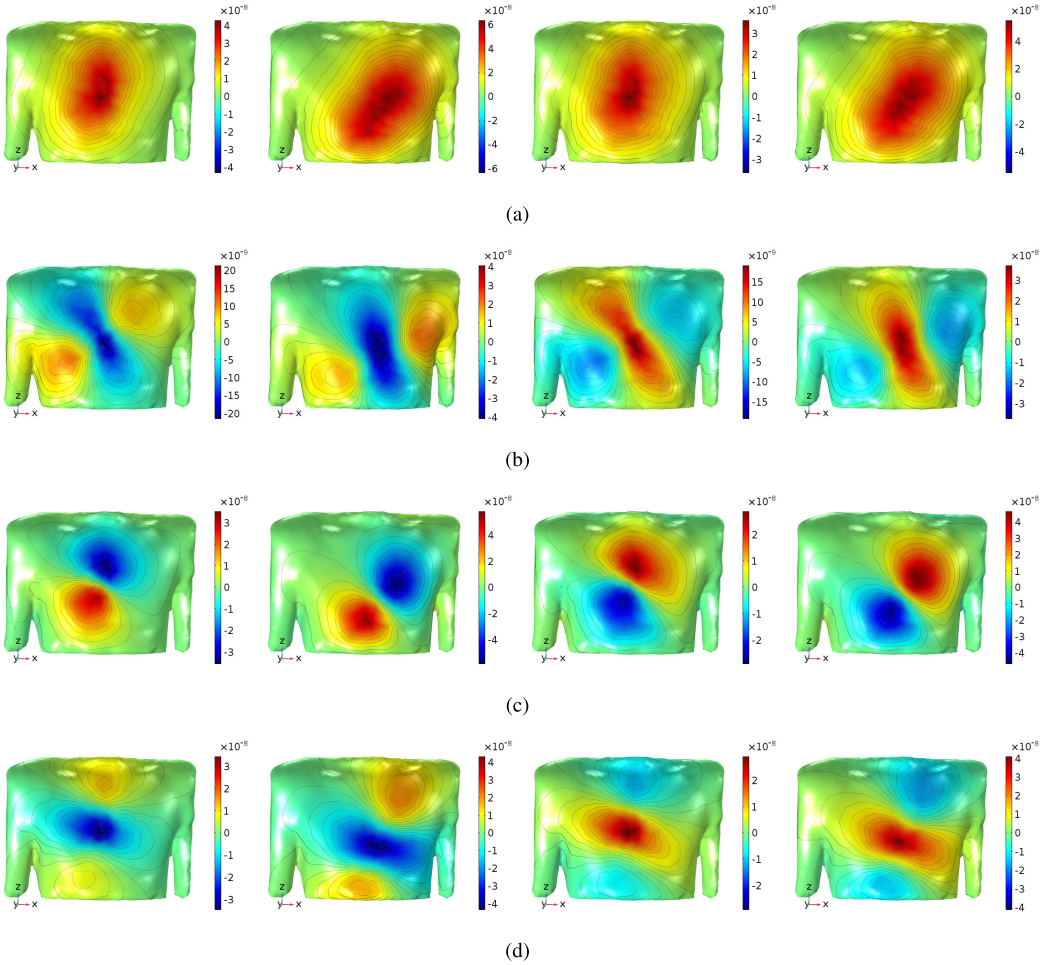

FIGURE 10. Simulated BSM distribution at four moments. Left to right: the depolarization process (t = 20, 40) and repolarization process (t = 120, 140). (a) The distribution of norm $|B|$. (b) The distribution in the direction parallel to body surface B_x. (c) In the direction perpendicular to body surface B_y. (d) In the direction parallel to body surface B_z.

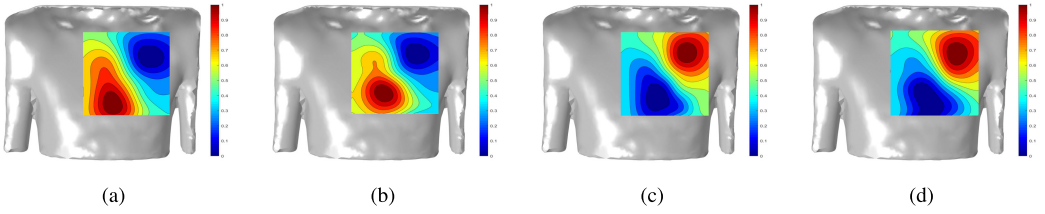

FIGURE 11. The BSM distribution in the B_y direction measured by our self-developed atomic magnetometer. (a) (b): Depolarization process. (c) (d): Repolarization process.

deviation is used as the contrast estimation, and the covariance is used as the measure of the structural similarity. The range of SSIM is −1 to 1. The closer the value to 1, the higher the similarity. In our comparison, SSIM of simulated MCGs and measured MCGs at the corresponding time were 0.70, 0.74, 0.70, 0.69, respectively.

It can be seen that both the simulated MCGs and the measured MCGs show a bipolar structure, and the positions of the two poles are deflected with the depolarization and repolarization of the heart, which was basically consistent with the measured MCGs in the literature [33]. However, there are some differences between the simulated MCGs and measured MCGs, as this study still has some shortcomings, for example, we did not consider the anisotropy of the heart tissue in the simulation process, which should be considered in our future work.

IV. CONCLUSION

In this paper, a forward computational framework that can be used to study the cardiac TMP propagation and the

distribution of BSM was constructed from a personalized 3D geometric model, to cardiac electrophysiological activity, to extracorporeal magnetic field. Compared with the current dipole model, the improved FHN equation is more consistent with the actual cardiac electrophysiological process as the basis of the cardiac electrophysiological diffusion model.

The framework of MCG forward problem was verified by analytical solutions. Firstly, the analytical solution of the simplified FHN equation was solved in 1D condition, which was compared with the numerical solution of Galerkin FEM under the same condition. Secondly, simplifying extracorporeal cardiac magnetic field model was a straight wire model, and the analytical solution of the magnetic induction intensity of the model was compared with the numerical solution. Through the error analysis of the above solutions, it has been proved that the framework is feasible. Finally, the accuracy of the framework was further verified by comparing the simulated MCGs with the actual MCGs measured on our self-developed pulse-pumped Rb atomic magnetometer.

The framework has good scalability. We can modify the parameters of the FHN equation or even the form of the FHN equation to simulate the abnormal magnetic field distribution caused by different cardiac TMPs in different diseases such as arrhythmia. In addition, by changing the locations of the cardiac pacemaker, it can be used to simulate the distribution of cardiac magnetic field in non-sinus rhythm conditions.

Studying the MCG forward problem has helped us to understand generation principles of MCG. It can also play an important role in assisting the clinical diagnosis of heart disease [34]. We can deduce the relationship between physiology and pathology of heart disease such as myocardial ischemia and arrhythmia from the response processes of cardiac conduction system. Although the model is not perfect, it has the advantages of lower computational costs while ensuring accuracy in solving the forward problem. This approach has laid a solid foundation for future analyses of the MCG inverse problem.

V. DISCUSSION

There are still some limitations of our framework. The simple heart-torso model ignored the diffusion tensor of cardiac fiber orientation, which has an important influence on the propagation of TMP [35], and the model did not accurately segment the specific morphology of each part, nor did it take the beating of heart into account.

In future work, we will take the beating of heart into account, and use a rule-based method to simulate fiber orientation to make the model closer to the real heart [36]. Then, we will determine the area and severity of ischemia from the medical images of a specific heart disease and obtain a more representative model and simulate the TMP distribution of a specific object [37]. Additionally, in our subsequent MCG inverse problem, we can use a epicardial surface potential distribution model based on Multivariate Adaptive Regression Splines (MARS) [38], [39] or Conic MARS (CMARS) or its robust version (RCMARS) to reduce the impact of modeling error on experiment, which performs well in ECG inverse problem [40], [41]. What's more, Conic Generalized Partial Linear Model (CGPLM) can be introduced to reduce the complexity of the model [42]. In our future studies on MCG inverse problem, these algorithms will provide guidance for us.

REFERENCES

[1] L. Y. Ma, W. Chen, R. Gao, L. Liu, M. L. Zhu, Y. Wang, Z. Wu, H. Li, D. Gu, Y. Yang, andd Z. Zheng, "China cardiovascular diseases report 2018: An updated summary," *J. Geriatric Cardiol.*, vol. 17, no. 1, p. 1, 2020.

[2] J. Lant, G. Stroink, B. ten Voorde, B. M. Horacek, and T. J. Montague, "Complementary nature of electrocardiographic and magnetocardiographic data in patients with ischemic heart disease," *J. Electrocardiol.*, vol. 23, no. 4, pp. 315–322, Oct. 1990.

[3] H. Zeng, J. Han, and X. Xin, "Research progress on the measurement of dielectric properties of biological tissues," *Chin. Med. Equip.*, vol. 4, no. 5, pp. 5–11, 2016.

[4] F. E. Smith, P. Langley, P. Van Leeuwen, B. Hailer, L. Trahms, U. Steinhoff, J. P. Bourke, and A. Murray, "Comparison of magnetocardiography and electrocardiography: A study of automatic measurement of dispersion of ventricular repolarization," *Europace*, vol. 8, no. 10, pp. 887–893, Oct. 2006.

[5] G. Bison, "Development of an optical cardio-magnetometer," Ph.D. dissertation, Univ. de Fribourg, Fribourg, Switzerland, 2004.

[6] D. Cohen, E. A. Edelsack, and J. E. Zimmerman, "Magnetocardiograms taken inside a shielded room with a superconducting point contact magnetometer," *Appl. Phys. Lett.*, vol. 16, no. 7, pp. 278–280, Apr. 1970.

[7] H. Xia, A. B.-A. Baranga, D. Hoffman, and M. V. Romalis, "Magnetoencephalography with an atomic magnetometer," *Appl. Phys. Lett.*, vol. 89, no. 21, Nov. 2006, Art. no. 211104.

[8] X. He, Y. Huang, S. Li, S. Su, W. Zheng, Z. Hu, and Q. Lin, "Human heart magnetism measurement based on atomic magnetometer," *Chin. J. Med. Phys.*, vol. 11, pp. 93–97, Nov. 2017.

[9] M. Bai, Y. Huang, G. Zhang, W. Zheng, Q. Lin, and Z. Hu, "Fast backward singular value decomposition (SVD) algorithm for magnetocardiographic signal reconstruction from pulsed atomic magnetometer data," *Opt. Exp.*, vol. 27, no. 21, pp. 29534–29546, 2019.

[10] G.-F. Shou, L. Xia, P. Ma, F.-K. Tang, and L. Dai, "Simulation study of a magnetocardiogram based on a virtual heart model: Effect of a cardiac equivalent source and a volume conductor," *Chin. Phys. B*, vol. 20, no. 3, Mar. 2011, Art. no. 030702.

[11] G. Shou, L. Xia, M. Jiang, and J. Dou, "Magnetocardiography simulation based on an electrodynamic heart model," *IEEE Trans. Magn.*, vol. 47, no. 9, pp. 2224–2230, Sep. 2011.

[12] E. A. P. Alday, C. Zhang, M. A. Colman, H. Ni, Z. Gan, and H. Zhang, "Comparison of electric- and magnetic-cardiograms produced by myocardial ischemia in models of the human ventricle and torso," in *Proc. Comput. Cardiol. Conf. (CinC)*, Sep. 2015, pp. 517–520.

[13] V. R. Bhat and H. Anitha, "Computational imaging of the cardiac activities using magnetocardiography," *J. Med. Eng. Technol.*, vol. 43, no. 7, pp. 401–410, Oct. 2019.

[14] R. Plonsey and D. Fleming, *Bioelectric Phenomena*. New York, NY, USA: McGraw-Hill, 1969.

[15] L. Zhao, "Research on medical image segmentation and 3D reconstruction algorithmm," Ph.D. dissertation, Shadong Univ., Jinan, China, 2008.

[16] G. Jiang, W. Qin, S. Zhou, and C. Wang, "Medical image segmentation and research status," *Chin. J. Comput.*, vol. 38, no. 6, pp. 1222–1242, 2015.

[17] R. R. Aliev and A. V. Panfilov, "A simple two-variable model of cardiac excitation," *Chaos, Solitons Fractals*, vol. 7, no. 3, pp. 293–301, Mar. 1996.

[18] R. FitzHugh, "Impulses and physiological states in theoretical models of nerve membrane," *Biophys. J.*, vol. 1, no. 6, pp. 445–466, 1961.

[19] L. Wang, H. Zhang, K. C. Wong, H. Liu, and P. Shi, "Physiological-model-constrained noninvasive reconstruction of volumetric myocardial transmembrane potentials," *IEEE Trans. Biomed. Eng.*, vol. 57, no. 2, pp. 296–315, Feb. 2010.

[20] A. M. Scher and A. C. Young, "Frequency analysis of the electrocardiogram," *Circulat. Res.*, vol. 8, no. 2, pp. 344–346, Mar. 1960.

[21] D. Geselowitz, "On the magnetic field generated outside an inhomogeneous volume conductor by internal current sources," *IEEE Trans. Magn.*, vol. MAG-6, no. 2, pp. 346–347, Jun. 1970.
[22] P. W. Partridge and C. A. Brebbia, *Dual Reciprocity Boundary Element Method*. Springer, 2012.
[23] J.-M. Jin, *The Finite Element Method Electromagnics*. Hoboken, NJ, USA: Wiley, 2015.
[24] H. Zhang and P. Shi, "A meshfree method for solving cardiac electrical propagation," in *Proc. 27th Annu. Conf. Eng. Med. Biol.*, 2005, pp. 349–352.
[25] C. Murphy and R. Lazzara, "Current concepts of anatomy and electrophysiology of the sinus node," *J. Interventional Cardiac Electrophysiol.*, vol. 46, no. 1, pp. 9–18, Jun. 2016.
[26] G. Fischer, B. Tilg, P. Wach, G. Lafer, and W. Rucker, "Analytical validation of the BEM—Application of the BEM to the electrocardiographic forward and inverse problem," *Comput. Methods Programs Biomed.*, vol. 55, no. 2, pp. 99–106, Feb. 1998.
[27] G. Griffiths and W. E. Schiesser, *Traveling Wave Analysis of Partial Differential Equations: Numerical and Analytical Methods With MATLAB and Maple*. New York, NY, USA: Academic, 2010.
[28] Z. Chen and J. Zhang, "Multiple traveling wave solutions and solitary wave solutions for fitzhugh-nagumo equation," *J. Henan Inst. Eng.*, vol. 22, no. 4, pp. 57–60, Dec. 2010.
[29] L. Wang, H. Zhang, K. C. Wong, H. Liu, and P. Shi, "Electrocardiographic simulation on personalised heart-torso structures using coupled meshfree-bem platform," *Int. J. Funct. Informat. Personalised Med.*, vol. 2, no. 2, pp. 175–200, 2009.
[30] S. Nattel, "New ideas about atrial fibrillation 50 years on," *Nature*, vol. 415, no. 6868, pp. 219–226, Jan. 2002.
[31] L. Wang, H. Zhang, K. Wong, H. Liu, and P. Shi, "Noninvasive imaging of 3D cardiac electrophysiology," in *Proc. 4th Int. Symp. Biomed. Imag., From Nano Macro*, 2007, pp. 632–635.
[32] Z. Wang, A. C. Bovik, H. R. Sheikh, and E. P. Simoncelli, "Image quality assessment: From error visibility to structural similarity," *IEEE Trans. Image Process.*, vol. 13, no. 4, pp. 600–612, Apr. 2004.
[33] G. Bison, N. Castagna, A. Hofer, P. Knowles, J.-L. Schenker, M. Kasprzak, H. Saudan, and A. Weis, "A room temperature 19-channel magnetic field mapping device for cardiac signals," *Appl. Phys. Lett.*, vol. 95, no. 17, 2009, Art. no. 173701.
[34] R. Fenici, D. Brisinda, and A. M. Meloni, "Clinical application of magnetocardiography," *Expert Rev. Mol. Diag.*, vol. 5, no. 3, pp. 291–313, May 2005.
[35] G. Seemann, D. Keller, D. Weiss, and O. Dossel, "Modeling human ventricular geometry and fiber orientation based on diffusion tensor MRI," in *Proc. Comput. Cardiol.*, 2006, pp. 801–804.
[36] R. Doste, D. S. Iglesias, G. Bernardino, A. Alcaine, R. Sebastian, S. G. Roisin, M. Sermesant, A. Berruezo, D. S. Quintana, and O. Camara, "A rule-based method to model myocardial fiber orientation in cardiac biventricular geometries with outflow tracts," *Int. J. Numer. Methods Biomed. Eng.*, vol. 35, no. 4, p. e3185, Apr. 2019.
[37] M. M. Seyedebrahimi and Y. Serinagaoglu, "Simulation of transmembrane potential propagation in normal and ischemic tissue using Aliev-Panfilov model," *Int. J. Biosci., Biochem. Bioinf.*, vol. 7, no. 1, p. 13, 2017.
[38] S. Kuter, Z. Akyurek, and G.-W. Weber, "Retrieval of fractional snow covered area from MODIS data by multivariate adaptive regression splines," *Remote Sens. Environ.*, vol. 205, pp. 236–252, Feb. 2018.
[39] A. Çevik, G.-W. Weber, B. M. Eyüboğlu, and K. K. Oğuz, "Voxel-MARS: A method for early detection of Alzheimer's disease by classification of structural brain MRI," *Ann. Oper. Res.*, vol. 258, no. 1, pp. 31–57, Nov. 2017.
[40] Ö. N. Onak, Y. S. Dogrusoz, and G. W. Weber, "Evaluation of multivariate adaptive non-parametric reduced-order model for solving the inverse electrocardiography problem: A simulation study," *Med. Biol. Eng. Comput.*, vol. 57, no. 5, pp. 967–993, May 2019.
[41] O. N. Onak, Y. S. Dogrusoz, and G. W. Weber, "Effects of measurement noise in MARS-based inverse ECG solution approach," in *Proc. 26th Signal Process. Commun. Appl. Conf. (SIU)*, May 2018, pp. 1–4.
[42] A. Özmen and G. W. Weber, "Robust conic generalized partial linear models using RCMARS method—A robustification of CGPLM," *AIP Conf. Proc.*, vol. 1499, no. 1, pp. 337–343, Nov. 2012.

ZHENGHUI HU received the Ph.D. degree from Zhejiang University, in 2005. He is currently a Professor with the College of Science, Zhejiang University of Technology. His research interest includes medical image processing.

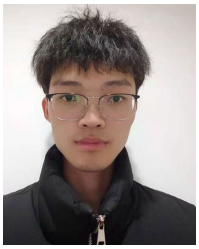

KAIKAI YE is currently pursuing the master's degree with the College of Science, Zhejiang University of Technology. His research interests include MCG signal processing and magnetocardiography classification.

MINGZHU BAI is currently pursuing the Graduate degree with the College of Science, Zhejiang University of Technology.

ZEKUAN YANG is currently pursuing the master's degree with the College of Science, Zhejiang University of Technology. His research interests include MCG signal processing and cardiac electrophysiological imaging.

QIANG LIN is currently a Professor and also the Dean of the College of Science, Zhejiang University of Technology. His research interests include quantum optics and precision measurement.